Airway Tree Segmentation for Optimal Stent Placement in Image-guided Radiotherapy

Ulrik L. Stephansen[1], Ronnie W. Horup[1], Mikkel Gram[1], Jens T. Olesen[1], Jesper Carl[2], Anne Sofie Korsager[1], and Lasse R. Østergaard[1]

[1] Department of Health Science and Technology, Aalborg University, Aalborg, Denmark
[2] Department of Medical Physics, Aalborg Hospital, Aarhus University, Aalborg, Denmark

Abstract. To reduce the target volume in image-guided radiotherapy it has been proposed to insert a removable thermo-expandable stent near the tumor, enabling the use of motion tracking and advanced gating techniques. An algorithm for extracting geometrical data on the airway tree from CT scans is presented, enabling clinicians to place a stent in close proximity to a lung tumor. The algorithm segments and skeletonizes the airway tree using wavefront propagation. Interpolated virtual slices are placed orthogonal on the skeleton, and the diameter is estimated using 2-D active contour modeling. The segmentation was compared to traditional region growing using seven CT scans of human lungs to validate the performance. The diameter estimation was validated using five phantom CT scans containing known diameters. Validation showed that wavefront propagation in general segmented a larger extent of the airway tree than region growing.

1 Introduction

According to the World Health Organization an estimated 1.61 million new cases of lung cancer are seen each year, making it the most common cancer in the world and the leading cause of cancer related deaths with an estimated 1.38 million deaths per year [1].

A commonly used treatment for lung cancer is image-guided radiotherapy, where CT scans are used to determine the planning target volume (PTV). This volume takes geometrical variations into account, e.g. respiratory motion, by adding a margin of up to 5 cm around the clinical target volume that it encloses. Consequently, a portion of normal tissue is included, making it hard to apply a conformal high dose to the cancerous tissue [2].

In order to compensate for target motion during radiotherapy, and thereby reduce the PTV, it is common to use either breath-hold technique, gating, or active tracking and dynamic delivery, also known as real-time tumor-tracking radiotherapy (RTRT) [2]. However, breath-holding can be difficult for lung cancer patients who often have a reduced pulmonary function, while gating requires coaching of the patient and a careful assessment of the respiratory motion [3].

Instead, recent studies have focused on the RTRT technique, in which the tumor is constantly tracked during radiotherapy using real-time X-rays adjusting the target area accordingly [4]. This can be done by either adjusting the couch on which the patient is placed, using the multileaf collimator (MLC) or a combination of both [2].

Various methods have been developed in order to track the tumor. In one study gold markers were placed near the tumor and tracked using an RTRT system, which only irradiated the tumor when the marker was within a specified region [4]. However, image noise and artifacts as well as air cavities and bone tissue have been shown to reduce the ability to successfully detect gold markers. New thermo-expandable stent markers have been developed and used for prostate cancer with the same accuracy as gold markers [5]. These stents could also be used for lung cancer and placed during bronchoscopy thus reducing the possibility of pneumothorax, a common complication of gold marker placement [6].

The aim of this article is to develop a method for accurate diameter estimation of the airway tree from CT data. A simple approach to segmentation of the airways is the traditional region growing algorithm, which utilizes the sharp contrast difference between bronchial walls and lumen [7]. However, it is subject to leaking if the bronchial wall is not continuous in the CT scan, e.g. in minor airways having thinner walls.

In this paper segmentation is performed using wavefront propagation, which is similar to region growing. However it is more local since the position of the wavefront(s) is always known, and thus leaks can be detected and confined without having to terminate the whole segmentation [8, 9]. The algorithm was chosen based on its robustness to leakage and ability to calculate a skeleton during segmentation [9, 10].

To estimate diameters with sub-voxel precision 2-D active contour modeling was used in combination with virtual re-slicing and tri-linear interpolation.

In the following the materials and methods used to develop and validate the algorithm are presented, followed by the results of the validation. Finally, the methods and results are discussed and a conclusion is made.

2 Materials and Methods

An algorithm was developed performing route planning in CT scans of human lungs. The algorithm extracts geometrical data in three steps:

1. Segmentation using wavefront propagation.
2. Virtual re-slicing and interpolation.
3. Diameter estimation using 2-D active contour modeling.

The wavefront propagation algorithm returns a segmentation and skeletonization of the airway tree. The skeleton is used for re-slicing and interpolation of the data in order to achieve accurate sub-voxel diameter estimates. The virtual slices are then used for estimating the diameter of the bronchi using 2-D active contour modeling.

2.1 Materials

A total of seven CT data sets were acquired from the Department of Medical Physics; Oncology and the Department of Respiratory Medicine at Aalborg Hospital for validation of the algorithm. The data ranged from 243 to 545 slices with a pixel spacing of 0.8008 to 0.9766 mm and a slice thickness of 0.625 to 1.25 mm. All CT scans had a matrix size of 512×512 pixels and a beam energy of 120 kVp.

Table 1. Key parameters describing test data resolution and image quality.

#	**No. slices**	**Avg. tube current** [mA]	**Pixel spacing** [mm]	**Slice thickness** [mm]
Human				
1	545	150.0	0.8008	0.625
2	243	30.2	0.9766	1.25
3	483	116.5	0.8750	0.625
4	463	220.0	0.9453	0.625
5	381	72.9	0.8926	0.625
6	439	35.8	0.9766	0.625
7	409	60.8	0.8320	0.625
Phantom				
8-12	64	380	0.6836	2.5

In addition to the CT data sets obtained from patients, a set of test phantom data from the National Biomedical Imaging Archive (NBIA) [11] was used for validating the diameter estimation. Each of the phantom CT series contained six cylinders with a diameter of approximately 3 mm (unknown tolerance). Phantom data contained 64 slices with a pixel spacing of 0.6836 mm and a slice thickness of 2.5 mm. For a more detailed description of the data used see Table 1.

2.2 Segmentation

Segmentation was performed using a wavefront propagation algorithm inspired by earlier implementations [8, 9, 10].

Wavefront propagation is a local version of region growing, propagating one segment at a time in a certain direction (Figure 1). The algorithm works using wavefronts, which are propagated in iterations. It is initiated with a threshold t and a seed voxel in the trachea forming the first wavefront. All non-segmented 18-connected neighbors having intensities lower than the threshold t constitute

the next wavefront, and the centroid of the wavefront is added to the skeleton. To add robustness to leakage, verification rules are implemented in the algorithm.

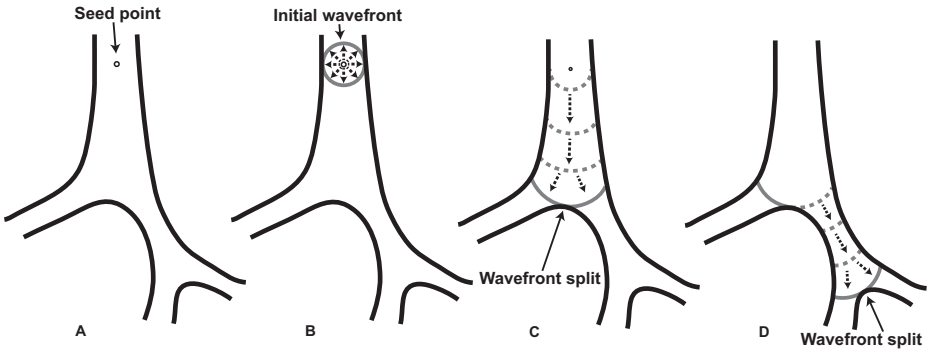

Fig. 1. The principle of wavefront propagation. A: The initial seed voxel in the trachea. B: The initial wavefront propagates in all directions away from the seed voxel until the trachea wall is reached, splitting the initial wavefront into two distinct connected components. C: Propagation of one of the new wavefronts created by the initial wavefront. The wavefront propagates until it is split at a bifurcation, creating two additional wavefronts. D: Propagation of the next wavefront further into the airway tree, until it reaches another bifurcation. The wavefront is then stopped and two new wavefronts are created. The process is repeated until all segments have been propagated.

Wavefront verification Each new wavefront is verified to determine if it is expanding too rapidly [8, 10]. The wavefront expansion ratio w_{exp} is calculated as the ratio between the number of voxels in the new wavefront $n\{\text{wavefront}\}$ and the initial wavefront $n\{\text{initial wavefront}\}$ of the segment:

$$w_{exp} = \frac{n\{\text{wavefront}\}}{n\{\text{initial wavefront}\}} \tag{1}$$

If w_{exp} exceeds the maximum allowed value $w_{exp_{max}}$ the newly formed wavefront is considered a leak and the whole segment is rejected. If a segment is rejected the threshold t is increased by Δg. The algorithm attempts to regrow the segment to segment as many airways as possible.

Segment verification Two verification rules are applied to completed segments. The first rule assumes child segments to be smaller than their parent segment [8, 10, 12, 13]. The segment expansion ratio s_{exp} is the ratio between the average number of voxels per propagation from the completed child segment and the parent segment:

$$s_{exp} = \frac{n\{\text{child}\}/N\{\text{child}\}}{n\{\text{parent}\}/N\{\text{parent}\}} \tag{2}$$

where $n\{\text{child}\}$ is the number of voxels in the child segment, and $N\{\text{child}\}$ is the number of wavefront propagations in the child segment. If s_{exp} exceeds the maximum allowed value $s_{exp_{max}}$ the completed segment is considered a leak and discarded, as well as any new wavefronts formed from the segment.

The second verification rule prunes the segmentation, as small and insignificant segments serve no purpose for the segmentation. Segments formed by only one or two wavefronts having no child segments are removed.

Post-processing After wavefront propagation is completed the skeleton is optimized. A child segment is merged with its parent if the parent segment has only got one child segment [8].

Finally a diameter is estimated for each segment using the volume and length of the segment, assuming it to be cylindrical. This information is used later during interpolation to specify the size of the interpolated plane.

2.3 Virtual re-slicing and interpolation

The next step of the algorithm was to re-slice and interpolate the data based on the segmented skeleton. This was done for two reasons:

1. The direction of the bronchi is not orthogonal to slices of the CT scan, which affects the cross section appearance.
2. The size of the bronchi can be as small as a few voxels, which entails very coarse diameter estimates due to limited image resolution.

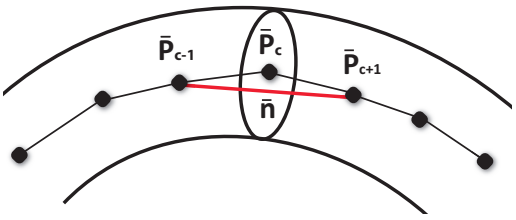

Fig. 2. 2-D view of a bronchus with corresponding skeleton. The red line is the normal vector $\boldsymbol{n}$ of the virtual plane and $\boldsymbol{P_c}$ is the current skeleton point and center of the virtual slice.

To accurately estimate the diameter of the bronchi the cross section must be orthogonal to the direction of the skeleton. This was ensured by creating a virtual slice in the CT volume perpendicular to the skeleton. The normal vector of the plane was calculated as the direction of the skeleton at the center point (Figure 2):

$$\boldsymbol{n} = \boldsymbol{P_{c-1}} - \boldsymbol{P_{c+1}} \tag{3}$$

A point on either side of the center point was chosen as the basis for the normal vector to give equal weight to the curvature of the bronchus around the center point.

The problem with very coarse resolution of small bronchi still remains. Therefore tri-linear interpolation of the plane was performed in order to estimate the diameter at sub-voxel level [14, 15]. An approximate diameter was calculated during segmentation, and the width of the virtual slice was defined dynamically as four times the approximate diameter. The interpolation resolution was defined as 101×101 pixels. Figure 3 shows a slice before and after interpolation.

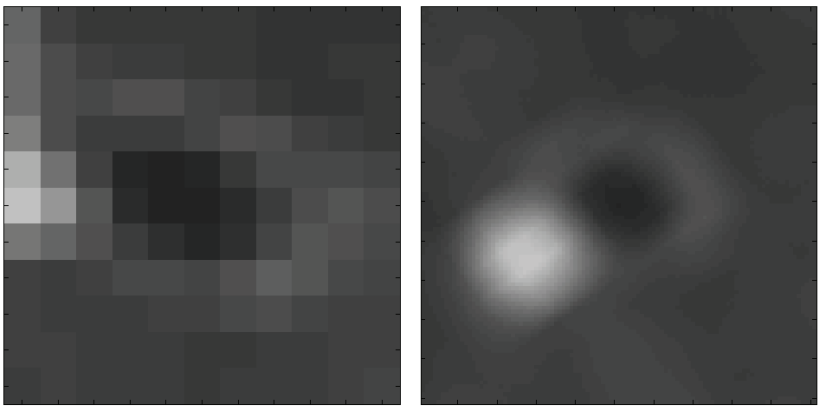

Fig. 3. View of the original slice containing a cross section of a bronchi and the interpolated plane normal to the direction of the skeleton. The rotation of the interpolated image is somewhat arbitrary, and the figures are not the exact same scale.

2.4 Diameter estimation

The bronchial diameter was estimated using 2-D active contour modeling based on the Chan-Vese formulation [16].

Tree major adaptations were made: Addition of a stop criteria, a contour validation step, and a diameter estimation function. The stop criteria was designed to exit the iterative process of minimization and return the contour if the difference in the length of the curve between two consecutive iterations was below a threshold of one thousandth the width of the virtual slice. Normally the process would continue a specified number of iterations.

In addition to the stop criteria the segmented contour was validated using a method first described by Mcnamara et al. [17], in which the airway contour roundness is determined. This was necessary as the skeleton from the wavefront propagation may have points placed within bifurcations, which would lead to an incorrect estimation of the diameter. The ratio d_r between the largest diameter d_l

within the contour and the largest diameter d_p perpendicular to it was calculated as:

$$d_r = \frac{d_l}{d_p} \tag{4}$$

If $d_r \geqslant 1.5$ the contour is discarded as it may be placed within a bifurcation or an oblique bronchus [17].

Following the validation process the diameter d was calculated assuming a circle of same circumference as the contour. This decision was based on the consideration that the bronchi can easily adapt to the circular shape of the stent. By running the algorithm on all the virtual slices an estimated diameter of the individual bronchial segments was obtained.

2.5 Validation

Route planning is dependent on the extent of the segmentation and accuracy of the diameter estimation. The performance and output of the algorithms was validated as described in the following.

Segmentation The segmentation algorithm was validated both quantitatively and qualitatively by comparison to traditional region growing [14]. In the region growing algorithm each voxel was added to the region if the absolute difference between the voxel intensity and the mean intensity of the region was below a certain threshold. The threshold was determined automatically for each data set using the highest threshold not causing excessive leakage.

To assess the degree of similarity between the segmented regions the Dice Similarity Coefficient (DSC) was calculated. The coefficient is a measure of the degree of overlap between two regions, and is defined as [18, 19]:

$$DSC = 2 \cdot \frac{n\{A \cap B\}}{n\{A\} + n\{B\}} \tag{5}$$

where A and B are the sets of segmented voxels using the two algorithms, and $n\{A\}$ is the number of elements in set A. Thus DSC is two times the ratio of the intersecting volume to the sum of the two volumes, and is within the range $[0, 1]$.

Diameter estimation The precision of the diameter estimation method was examined using five phantom data sets. In each series three cylinders were skeletonized as shown in Figure 4 and one cylinder was skeletonized using wavefront propagation with a manually located seed point.

The first two methods of skeletonization were used to determine how the active contour method performs if the extracted skeleton deviated from the ideal skeleton of the volume. The third skeletonization was created to test the robustness of the diameter estimation method by subjecting it to virtual slices with an oblique angle caused by the unstructured manual point placement. The fourth skeletonization was made in order evaluate the performance in the practical application.

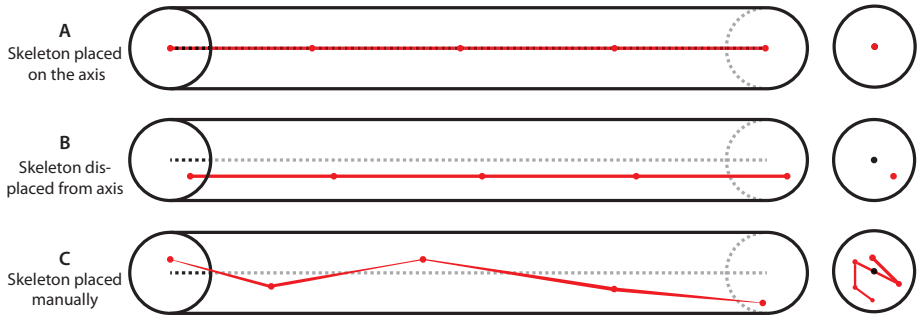

Fig. 4. Side and end view of the three types of skeletons placed within the hollow cylinders. A: Five consecutive points on the axis of the volume. B: As in A, but displaced from the axis. C: Five points manually selected with the intention of creating an unstructured skeleton.

3 Results

3.1 Segmentation

The developed segmentation algorithm was compared to a traditional 3-D region growing algorithm. Results from the quantitative validation of the segmentation algorithm are shown in Table 2. The values for wavefront propagation were obtained using $t = -820$ HU, $w_{exp_{max}} = 2.8$, $s_{exp_{max}} = 1.5$, $\Delta g = -10$ HU, which yielded the best results.

Table 2. Segmented volume of each image sequence using adaptive region growing (RG) and wavefront propagation (WP). The increase in volume using wavefront propagation compared to region growing and Dice Similarity Coefficient (DSC) is also listed.

#	**Vol. (RG)** [mm^3]	**Vol. (WP)** [mm^3]	**Increase**	**DSC**
1	37,889	46,814	23.6%	0.893
2	31,599	36,617	15.9%	0.926
3	38,748	57,581	48.6%	0.804
4	55,450	55,092	−0.6%	0.986
5	22,283	30,667	37.6%	0.821
6	29,913	27,394	−8.4%	0.945
7	25,983	35,286	35.8%	0.847

The results show a positive correlation between tube current ($\sim$ dose) and segmented volume (correlation 0.80 using region growing; 0.87 using wavefront propagation).

During the qualitative validation three major areas were found in which the region growing and the wavefront propagation differed. These were:

- Spongy holes in the segmentation (false negatives on voxel level).
- Leakage into the lungs (false positives).
- Missed bronchi (false negatives on branch level).

Segmented regions are shown in Figure 5.

Wavefront propagation completed in a median time of 21.3 seconds (min 11.2 seconds, max 45.2 seconds) per CT scan using a 2.2 GHz Intel Core 2 Duo 64 bit system having 4 GB 667 MHz DDR2 RAM.

3.2 Diameter estimation

Results of the validation are shown in Table 3. One diameter estimate was discarded from the manual skeleton by the validation step of the algorithm. The active contour diameter estimation completed in a median time of 537.4 seconds (or 8.96 minutes) per CT scan (min 5.00 minutes, max 18.33 minutes) using the same system as during wavefront propagation.

Table 3. Results from validation of diameter estimation using active contours. The method was applied to the four skeletons; 'Axis', 'Displaced', 'Manual' and 'Wavefront', of which the later is the skeleton created during wavefront propagation. Values in millimeters. Correct diameter was approximately 3 mm. *One estimate removed by ACM validation.

	Axis	**Displaced**	**Manual**	**Wavefront**
Mean	3.32	3.20	3.12∗	3.09
STD	0.02	0.12	0.07	0.11

4 Conclusion

The ability to automatically segment and calculate the dimensions of the airway tree may prove to be a valuable tool for stent placement and choosing the correct stent size, enabling planning target volume reduction within image-guided radiotherapy of lung cancer.

Results showed that wavefront propagation provided a fast segmentation and skeletonization of the human airway tree in seven CT image series. Also, the estimation of the bronchial diameters using 2-D active contour modeling proved to be a reliable method when applied to phantom CT scans with known dimensions, and proved to be robust to imperfections in the skeleton.

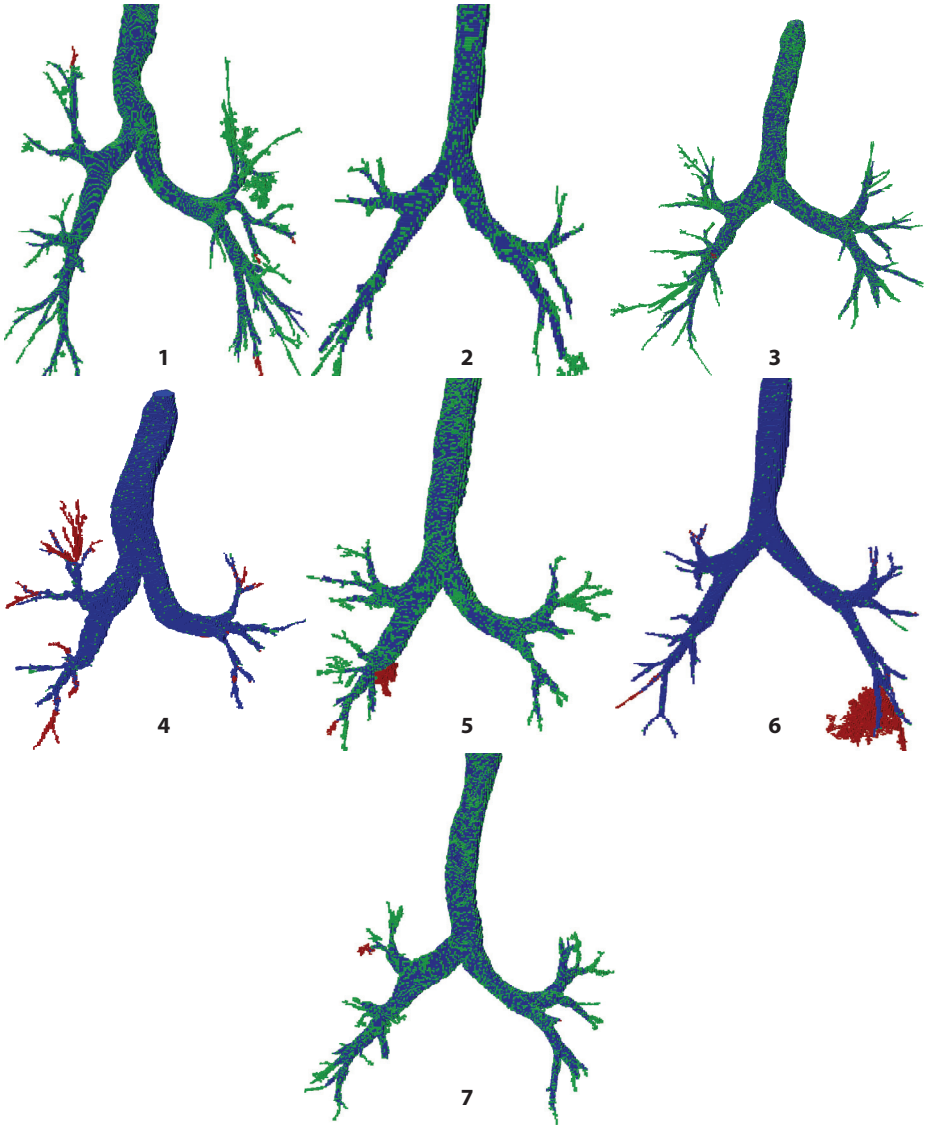

Fig. 5. Results from segmentation of the seven human subjects using region growing and wavefront propagation. Blue denotes areas segmented by both algorithms, green denotes areas segmented only by wavefront propagation, and red denotes areas segmented only by region growing.

Bibliography

[1] J. Ferlay, H. R. Shin, F. Bray, D. Forman, C. Mathers, and D. M. Parkin. GLOBOCAN 2008, cancer incidence and mortality worldwide: IARC CancerBase no. 10, 2010. URL `http://globocan.iarc.fr`.

[2] I. Buzurovic, K. Huang, Y. Yu, and T. K. Podder. A robotic approach to 4D real-time tumor tracking for radiotherapy. *Phys Med Biol*, 56(5):1299–1318, Mar 2011.

[3] C. Saw, E. Brandner, R. Selvaraj, H. Chen, M. Saiful Huq, and D. Heron. A review on the clinical implementation of respiratory-gated radiation therapy. *Biomed Imaging Interv J*, 3(1), 1 2007. doi: 10.2349/biij.3.1.e40.

[4] H. Shirato, S. Shimizu, K. Kitamura, and R. Onimaru. Organ motion in image-guided radiotherapy: lessons from real-time tumor-tracking radiotherapy. *Int J Clin Oncol*, 12(1):8–16, Feb 2007.

[5] J. Carl, H. Nielsen, J. Nielsen, B. Lund, and E. H. Larsen. Automated detection of a prostate Ni–Ti stent in electronic portal images. *Medical Physics*, 33(12):4600–4605, December 2006. doi: 10.1118/1.2369466.

[6] R. I. Whyte, R. Crownover, M. J. Murphy, D. P. Martin, T. W. Rice, M. M. DeCamp, R. Rodebaugh, M. S. Weinhous, and Q. T. Le. Stereotactic radiosurgery for lung tumors: preliminary report of a phase i trial. *Ann Thorac Surg*, 75(4):1097–1101, Apr 2003.

[7] S. A. Wood, E. A. Zerhouni, J. D. Hoford, and E. A. Hoffman. Measurement of three-dimensional lung tree structures by using computed tomography. *Journal of Applied Physiology*, 79(5):1687–1697, November 1995.

[8] B. van Ginneken, W. Baggerman, and E. van Rikxoort. Robust segmentation and anatomical labeling of the airway tree from thoracic CT scans. In Dimitris Metaxas, Leon Axel, Gabor Fichtinger, and Gábor Székely, editors, *Medical Image Computing and Computer-Assisted Intervention – MICCAI 2008*, volume 5241 of *Lecture Notes in Computer Science*, pages 219–226. Springer Berlin / Heidelberg, 2008. doi: 10.1007/978-3-540-85988-8_27.

[9] T. Schlathölter, C. Lorenz, I. C. Carlsena, S. Renischa, and T. Deschamps. Simultaneous segmentation and tree reconstruction of the airways for virtual bronchoscopy. *Proceedings of SPIE*, 4684:103–113, 2002.

[10] T. Bülow, C. Lorenz, and S. Renisch. A general framework for tree segmentation and reconstruction from medical volume data. In Christian Barillot, David R. Haynor, and Pierre Hellier, editors, *Medical Image Computing and Computer-Assisted Intervention – MICCAI 2004*, volume 3216 of *Lecture Notes in Computer Science*, pages 533–540. Springer Berlin / Heidelberg, 2004. doi: 10.1007/978-3-540-30135-6_65.

[11] U. S. National Institutes of Health. National biomedical imaging archive, 2011. URL `https://imaging.nci.nih.gov/`.

[12] J. A. Verschakelen and W. de Wever. *Computed Tomography of the Lung A Pattern Approach*. Springer, 2007. doi: 10.1007/978-3-540-68260-8.

[13] K. Horsfield, F. G. Relea, and G. Cumming. Diameter, length and branching ratios in the bronchial tree. *Respiration Physiology*, 26:351–356, 1976.

[14] J. Toriwaki and H. Yoshida. *Fundamentals of Three-Dimensional Digital Image Processing*. Springer, 2009.

[15] R. W. Parrott, M. R. Stytz, P. Amburn, and D. Robinson. Towards statistically optimal interpolation for 3-D medical imaging. *IEEE Engineering in Medicine and Biology*, pages 49–59, 1993.

[16] T. F. Chan and L. A. Vese. Active contours without edges. *IEEE Transactions on Image Processing*, 10(2):266–277, 2001.

[17] A. E. Mcnamara, N. L. Müller, M. Okazawa, J. Arntorp, B. R. Wiggs, and P. D. Paré. Airway narrowing in excised canine lungs measured by high-resolution computed tomography. *J Appl Physiol*, 73:307–316, 1992.

[18] A. P. Zijdenbos, B. M. Dawant, R. A. Margolin, and A. C. Palmer. Morphometric analysis of white matter lesions in MR images: method and validation. *IEEE Trans Med Imaging*, 13(4):716–724, 1994. doi: 10.1109/42.363096.

[19] K. H. Zou, S. K. Warfield, A. Bharatha, C. M. Tempany, M. R. Kaus, S. J. Haker, W. M. Wells, F. A. Jolesz, and R. Kikinis. Statistical validation of image segmentation quality based on a spatial overlap index. *Acad Radiol*, 11(2):178–189, Feb 2004.